

LIFE CYCLE OF TURBULENT KINETIC ENERGY IN RAYLEIGH-BÉNARD CONVECTION AT MODERATE Ra

Myoungkyu Lee

Department of Aerospace Engineering and Mechanics
The University of Alabama
Tuscaloosa, AL 35487, USA
mkleee@ua.edu

ABSTRACT

The life-cycle of turbulent kinetic energy (TKE) in the canonical Rayleigh-Bénard flows is investigated. The spectral densities of terms in the TKE budget equation are computed with direct numerical simulations (DNSs) at Rayleigh numbers, Ra , up to 4×10^8 . The result exhibits that both production and dissipations are most significant at the center between two planes. Small-scale motions are dominant for dissipation, while the non-negligible amount of TKE is dissipated by large-scale motions in the near-wall region. On the other hand, large-scale motions are dominant for the production of TKE, but small-scale motions also contribute to the production of TKE. It suggests that the traditional energy cascade model, which describes the energy transfer from large-scale to small-scale, has a significant role in the life-cycle of TKE. Furthermore, the cascade process from large-scale motion to small-scale motion involves transports by nonlinear mechanisms, such as turbulence and pressure-velocity correlations. The length-scale of the wall-normal transport mechanism in the overlap region grows linearly with wall-normal distances, and such linear growth regions increase with Ra .

INTRODUCTION

The super-structure or very large-scale motions (VLSMs) of turbulent flows are observed in various types of wall-bounded turbulence. Such large-scale motions are stronger in boundary-driven wall-bounded turbulence than in pressure-gradient-driven wall-bounded turbulences (Lee & Moser, 2015; Pandey *et al.*, 2018; Lee & Moser, 2018). Rayleigh-Bénard convective flow is another boundary condition driven flow with VLSMs (Stevens *et al.*, 2018; Krug *et al.*, 2020; Green *et al.*, 2020; Blass *et al.*, 2021). The large-scale motions (LSMs) of Rayleigh-Bénard convective flows are important in various engineering and scientific problems, e.g., atmospheric flows, boiling devices, etc., since they govern the macroscopic transport of mass and turbulent kinetic energies (Ahlers *et al.*, 2009).

Recently, some properties of the large-scale motions in Rayleigh-Bénard convective flows have been revealed by several DNS studies. The TKE spectral densities at different Ra have peaks at $k = 1$ where k is the circular wavenumber (Stevens *et al.*, 2018), and the size of large-scale motions grow with Ra (Krug *et al.*, 2020). Krug *et al.* also reported that the size of large-scale structures in the temperature field is different from the size of large-scale motions in vertical velocity fields, and the difference is strongly connected to the pro-

duction mechanism of vertical velocity fluctuations. Yet, the understanding of the life-cycle of large-scale motions is still incomplete. The objective of the current work is to study the life-cycle of TKE in Rayleigh-Bénard convective flows.

In this work, we investigate the terms in the TKE budget equation in terms of length-scale and wall-normal locations to understand the life-cycle of TKE in Rayleigh-Bénard convection problems at different Ra s. Among numerous earlier works in this context, we highlight a few works. (Deardorff & Willis, 1967) performed TKE budget analysis with the flows up to $Ra = 2.5 \times 10^6$. Kerr (2001) studied the effect of aspect ratio on the TKE dissipation. More recently, Krug *et al.* (2020) performed the spectral analysis on the production of TKE and revealed the importance of LSMs in Rayleigh-Bénard convection at high Ra . Separately, Lee & Moser (2019) performed spectral analysis of the budget equations of velocity variances with DNS of channel flow at high Re . The same spectral analysis technique is used for this study and summarized in the next section.

METHOD

DNSs of the incompressible Rayleigh-Bénard convection are performed for this study. We solve the normalized governing equations for the incompressible Rayleigh-Bénard convection. Those are

$$\begin{aligned} \frac{\partial u_k}{\partial x_k} &= 0 \\ \frac{\partial u_i}{\partial t} &= -\frac{\partial u_i u_k}{\partial x_k} + \sqrt{\frac{Pr}{Ra}} \frac{\partial^2 u_i}{\partial x_k \partial x_k} - \frac{\partial p}{\partial x_i} + \theta \delta_{i3} \\ \frac{\partial \theta}{\partial t} &= -\frac{\partial \theta u_k}{\partial x_k} + \frac{1}{\sqrt{Pr Ra}} \frac{\partial^2 \theta}{\partial x_k \partial x_k} \end{aligned} \quad (1)$$

where Pr and Ra are Prandtl number and Rayleigh number, respectively. Also, u_i , p , θ and δ_{ij} are the velocity components, pressure, normalized temperature and Kronecker's delta, respectively. x_1 and x_2 are homogeneous directions, and x_3 is the wall-normal direction. No-slip and no-penetration conditions for velocity fields are applied at top and bottom walls. Boundary conditions for normalized temperatures are

$$\theta_{x_3=0} = \frac{1}{2}, \quad \theta_{x_3=h} = -\frac{1}{2} \quad (2)$$

Case	Ra	L/H	N_{\parallel}	N_{\perp}	Nu	Re_{\parallel}	Re_{\perp}	Re_T	δ_{θ}
1E5	1×10^5	10π	512	96	4.34	55.6	40.1	68.6	1.152×10^{-1}
6E6	6×10^6	5π	768	256	13.62	425.3	299.4	520.1	3.672×10^{-2}
4E8	4×10^8	5π	2048	512	46.37	3141.7	1962.4	3704.3	1.078×10^{-2}

Table 1. Simulation parameters. L : simulation domain size in the homogeneous directions, H : distance between walls, N_{\parallel} : number of grid points in spectral domain, N_{\perp} : number of collocation points in wall-normal direction, Re_{\parallel} : horizontal Reynolds number, Re_{\perp} : wall-normal Reynolds number, Re_T : total Reynolds number, δ_{θ} : thermal boundary layer thickness

where h is the distance between two walls. We use the velocity-vorticity formulation from Kim *et al.* (1987). Spectral-Galerkin method and seventh-order basis spline-collocation method is used for derivatives in homogeneous and the wall-normal directions, respectively. Orszag's 3/2 rules are applied with zero padding to remove the aliasing for computing quadratic products (Orszag, 1971). The low-storage third order Runge-Kutta method is used for the time integration. Modified in-house simulation code, which has been used for Lee & Moser (2015, 2018), is used for simulations. Consult Lee *et al.* (2013, 2014) for details of the simulation code implementations.

We simulate three cases at different Ras with fixed Pr , $Pr = 1$. The Nusselt number, Nu and thermal boundary layer thickness, δ_{θ} , of three cases are in table 1. The values in table 1 agrees values from Krug *et al.* (2020) within statistical uncertainties.

The two-point correlation function corresponding to the turbulent kinetic energy (TKE, $K = \langle u_i u_i \rangle / 2$) is defined with quantities separated in homogeneous directions, \mathbf{r} , e.g. $\tilde{u}_i = u_i(\mathbf{x} + \mathbf{r})$ where $\mathbf{x} = (x_1, x_2, x_3)$ and $\mathbf{r} = (r_1, r_2, 0)$.

$$2\mathcal{R}_K(r_1, r_2, x_3) = \langle u'_i \tilde{u}'_i \rangle \quad (3)$$

where $\langle \cdot \rangle$ denotes the averaging in time and homogeneous directions. With some mathematical manipulations, the budget equation of \mathcal{R}_K is obtained as follows.

$$\frac{\partial \mathcal{R}_K}{\partial t} = \mathcal{R}_P + \mathcal{R}_T^{\parallel} + \mathcal{R}_T^{\perp} + \mathcal{R}_{\Pi} + \mathcal{R}_D - \mathcal{R}_{\varepsilon} \quad (4)$$

where

$$\begin{aligned} 2\mathcal{R}_P &= \langle u'_3 \tilde{\theta}' \rangle + \langle \tilde{u}'_3 \theta' \rangle \\ 2\mathcal{R}_T^{\perp} &= -\frac{1}{2} \left(\frac{\partial \langle \tilde{u}'_i u'_i u'_3 \rangle}{\partial x_3} + \frac{\partial \langle u'_i \tilde{u}'_i \tilde{u}'_3 \rangle}{\partial x_3} \right) \\ 2\mathcal{R}_{\Pi} &= \frac{\partial \langle u'_3 \tilde{p}' \rangle}{\partial x_3} + \frac{\partial \langle \tilde{u}'_3 p' \rangle}{\partial x_3} \\ 2\mathcal{R}_D &= \sqrt{\frac{Pr}{Ra}} \frac{\partial^2 \langle u'_i \tilde{u}'_i \rangle}{\partial x_3^2} \end{aligned}$$

$$\begin{aligned} 2\mathcal{R}_T^{\parallel} &= \frac{\partial \langle \tilde{u}'_i u'_i u'_1 \rangle}{\partial r_1} - \frac{\partial \langle u'_i \tilde{u}'_i \tilde{u}'_1 \rangle}{\partial r_1} + \frac{\partial \langle \tilde{u}'_i u'_i u'_2 \rangle}{\partial r_2} - \frac{\partial \langle u'_i \tilde{u}'_i \tilde{u}'_2 \rangle}{\partial r_2} \\ &\quad - \frac{1}{2} \left(\frac{\partial \langle \tilde{u}'_i u'_i u'_3 \rangle}{\partial x_3} + \frac{\partial \langle u'_i \tilde{u}'_i \tilde{u}'_3 \rangle}{\partial x_3} \right) \\ &\quad + \left\langle \tilde{u}'_i \tilde{u}'_3 \frac{\partial u'_i}{\partial x_3} \right\rangle + \left\langle u'_i u'_3 \frac{\partial \tilde{u}'_i}{\partial x_3} \right\rangle \\ 2\mathcal{R}_{\varepsilon} &= \sqrt{\frac{Pr}{Ra}} \left(\frac{\partial \langle u'_i \tilde{u}'_i \rangle}{\partial r_1^2} + \frac{\partial \langle u'_i \tilde{u}'_i \rangle}{\partial r_2^2} + \left\langle \frac{\partial u'_i}{\partial x_3} \frac{\partial \tilde{u}'_i}{\partial x_3} \right\rangle \right) \end{aligned}$$

The Fourier transforms of terms in (4) with respect to the separation distances provide spectral densities of terms in the TKE budget equation.

$$\frac{\partial E_K}{\partial t} = E_P + E_T^{\parallel} + E_T^{\perp} + E_{\Pi} + E_D - E_{\varepsilon} \quad (5)$$

The integration of terms in (5) over k_1 and k_2 are the terms in the TKE budget equations (Deardorff & Willis, 1967).

$$\frac{\partial K}{\partial t} = P + T + \Pi + D - \varepsilon \quad (6)$$

where P , T , Π , D and ε are production, wall-normal transport by turbulence, wall-normal transport by pressure-velocity interaction, wall-normal transport by viscosity and dissipation, respectively. Note that the integration of E_T^{\parallel} over k_1 and k_2 is zero.

$$\lim_{\substack{r_1 \rightarrow 0 \\ r_2 \rightarrow 0}} \mathcal{R}_T^{\parallel} = \int_{-\infty}^{\infty} \int_{-\infty}^{\infty} E_T^{\parallel} dk_1 dk_2 = 0, \quad \forall x_3 \quad (7)$$

Therefore, we interpret E_T^{\parallel} as the term for inter-scale transfer at any fixed wall-normal distance, and this term is not shown in the TKE budget equation, eq (6). Also, both T and Π are wall-normal transport terms with nonlinear interaction of velocity components, while D is the linear wall-normal transport terms. Note that the pressure field in incompressible flows is the result of nonlinear interactions of velocity components to satisfy the divergence-free condition. Therefore, we combine T and Π as follows.

$$\mathcal{N} = T + \Pi \quad (8)$$

and

$$E_{\mathcal{N}} = E_T^{\perp} + E_{\Pi} \quad (9)$$

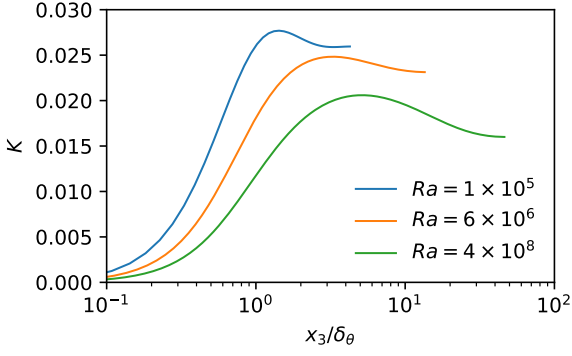


Figure 1. One-dimensional profile of turbulent kinetic energy (TKE)

Note that integration of $E_{\mathcal{N}}$ or E_D over x_3 at any wavenumber is zero.

$$\int_0^{h/2} E_{\mathcal{N}} dx_3 = \int_0^{h/2} E_D dx_3 = 0, \quad \forall(k_1, k_2) \quad (10)$$

Finally,

$$\frac{\partial E_K}{\partial t} = E_P + E_T^{\parallel} + E_{\mathcal{N}} + E_D - E_{\varepsilon} \quad (11)$$

RESULT

In this section, the profile and spectral density of TKE are discussed. Then, its budget terms are discussed in the order of production, dissipation, linear wall-normal transport, nonlinear wall-normal transport, and inter-scale transfer.

The one-dimensional profile of TKE is shown in the figure 1. Locations of TKE peaks increase with Ra , while the values of TKE peaks decrease with Ra . Also, the increasing rate of TKE at the near-wall region exhibit some Ra dependencies. Corresponding one-dimensional spectral densities of TKE are shown in the figure 2. Note that figures with spectral densities are represented as functions of k and x_3/δ_θ . k is premultiplied to all spectral densities to compensate for the log scales in k domains. The premultiplied TKE spectra shows strong peak at $x_3/\delta_\theta = 1$ and $\lambda/\delta_\theta = 40$ ($\lambda/h \approx 4.5$) at $Ra = 1 \times 10^5$. Interestingly, LSMs at $Ra = 6 \times 10^6$ show bimodal peaks, and the peaks show scale separations as Ra increases. It is possible that this observation is an artifact of arbitrary bin size to obtain the spectral density in k with $\Delta k = 0.5$. There is only one more data point between two peaks at $Ra = 6 \times 10^6$, but there are two data points between two peaks at $Ra = 4 \times 10^8$. Nonetheless, the data confirms that the length-scale of superstructure rolls grows with Ra , which is consistent with (Pandey *et al.*, 2018). Additional simulation results with much bigger simulation domains at higher Ra are necessary to verify this observation, but the costs of such simulations are prohibitively expensive.

One-dimensional profiles of production and dissipation of TKE in figure 3 show that most of the produced TKE get dissipated at the same wall-normal locations, and a small portion of TKE which is not dissipated in the outer region is dissipated at the near-wall region, $x_3/\delta_\theta < 1$. Here, x_3/δ_θ is also premultiplied to the budget terms to compensate the log-scale in x_3/δ_θ similar to k -premultiplied spectral density of TKE. The imbalance between production and dissipation is more vivid in the

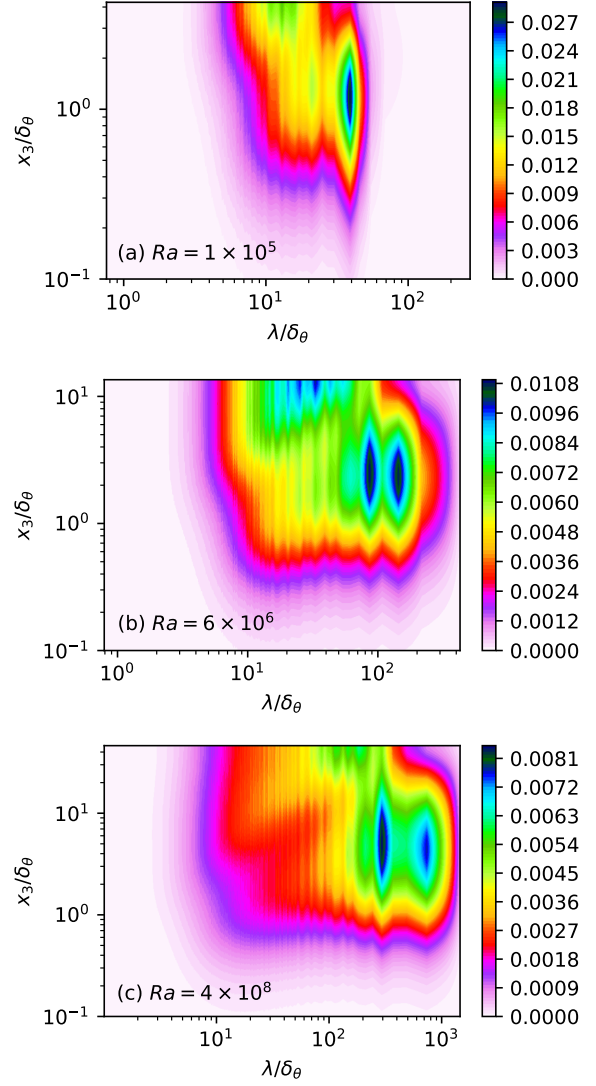


Figure 2. k -Premultiplied spectral densities of TKE

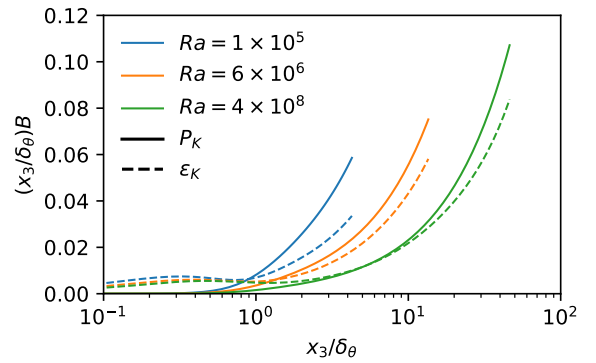


Figure 3. One-dimensional profile of TKE production (P_K) and dissipation (ε_K)

spectral density of those. The spectral densities of production have peaks at the middle point between walls, and corresponding length-scales of peaks increase with Ra even with outer scaling, λ/h . Similarly, the spectral densities of dissipation have peaks at the middle point between walls. However, the length-scale of dominant dissipation is $\lambda/\delta_\theta = 7 - 8$ and it is

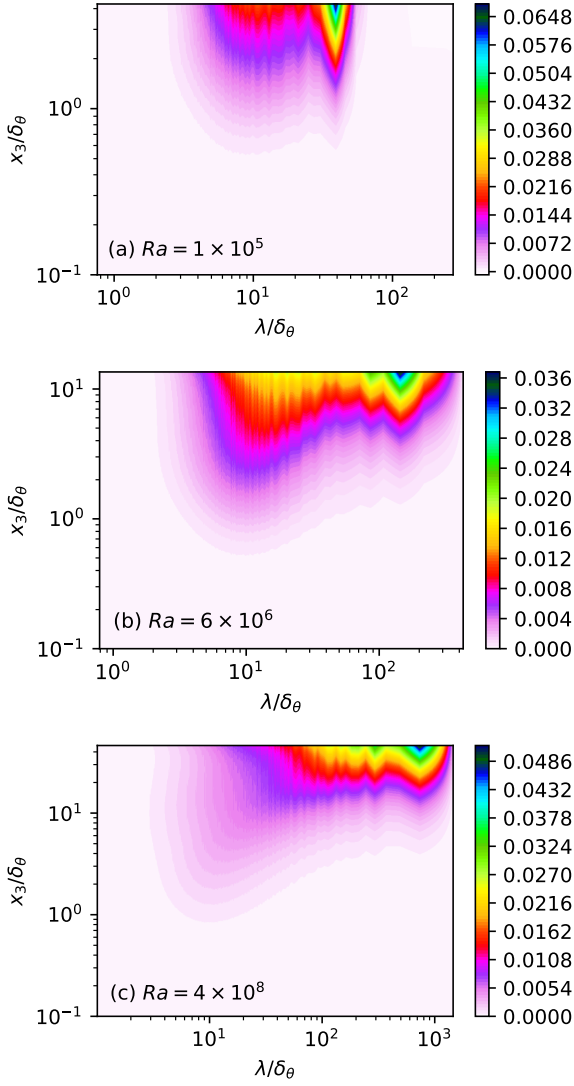


Figure 4. k - and x_3 -Premultiplied spectral density of P_K

almost invariant to Ra . Interestingly, a small amount is dissipated at the near-wall region, and their length-scale is consistent with the large-scale structure of production. The different spectral behaviors of production and dissipation imply that the roles of wall-normal transport mechanisms and inter-scale transfer are important in the life-cycle of TKE.

Figure 6 shows that the non-linear wall-normal mechanism transports TKE from the outer region to the near-wall region. Then, the linear wall-normal mechanism transports TKE further to the wall. However, the spectral behaviors of wall-normal transport mechanisms are more complex. The observation with one-dimensional profiles still holds with large-scale motions. (Figure 7) When the length scale gets smaller, the nonlinear wall-normal mechanism also transports some TKE away from the wall. Also, the length scale of the donor region in the nonlinear mechanism linearly increases with wall-normal distance, $\lambda \sim x_3$, and this linear growth is vivid when Ra increases. There is a small region where the linear mechanism also transports TKE away from the wall (Figure 8). This behavior is only shown in the region $x_3/\delta_\theta > 1$, and the magnitude is negligible. Generally, the linear mechanism transports TKE, which is transported from the outer region by the nonlinear mechanism, to the near-wall region in all length scales.

The spectral behavior of inter-scale TKE transfer is shown

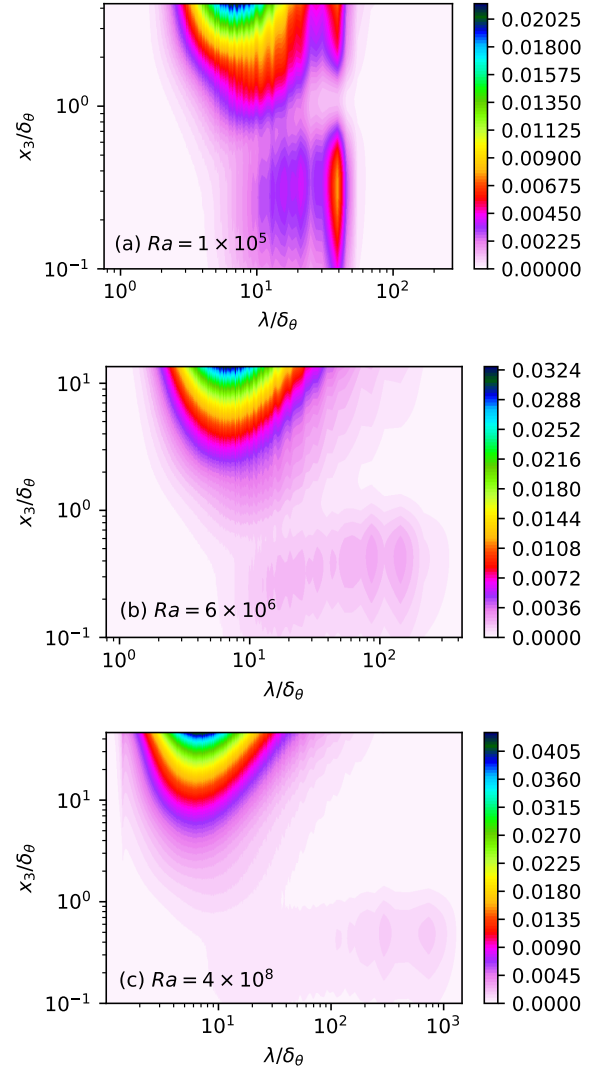


Figure 5. k - and x_3 -Premultiplied spectral density of ϵ_K

in figure 9. At $Ra = 1 \times 10^5$, the strong donor region is where the production spectra show the peak. A small inverse energy cascade is observed in the near-wall region at $Ra = 1 \times 10^5$, but the magnitude of the inverse TKE cascade is small. Also, the inverse energy cascade is not observed at higher Ra flows. The inter-scale transfer mechanism in the outer region, say $x_3/h > 0.1$, shows different behavior from the near-wall region. The donor region has only one peak at $Ra = 1 \times 10^5$. However, two peaks are observed in the donor region at outer flow in higher Ra flows, while the recipient region has a single peak in all flows. Among the peaks in the donor region at high Ra flows, the peak with larger-scale is at the same length-scale where the production mechanism has peaked. However, the peaks at the intermediate length scale are at different length scales where the production spectra have peaks. Instead, the TKE transferred from the intermediate length scale is from the region closer to the wall. The TKE produced at the large-scale motion at the middle point between walls transported toward walls, say $x_3/h < 0.1$ by the nonlinear wall-normal transport mechanism. Then, the inter-scale mechanism transfers the energy from the large-scale to the intermediate length scale. Finally, the nonlinear wall-normal mechanism transports TKE toward the middle point between walls at a given length scale.

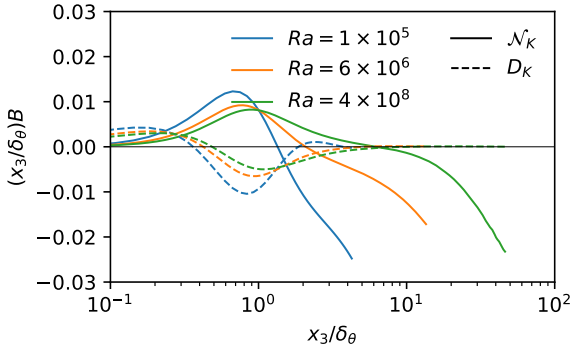


Figure 6. One-dimensional profile of nonlinear wall-normal transport of TKE (\mathcal{N}_K), and linear wall-normal transport of TKE (D_K).

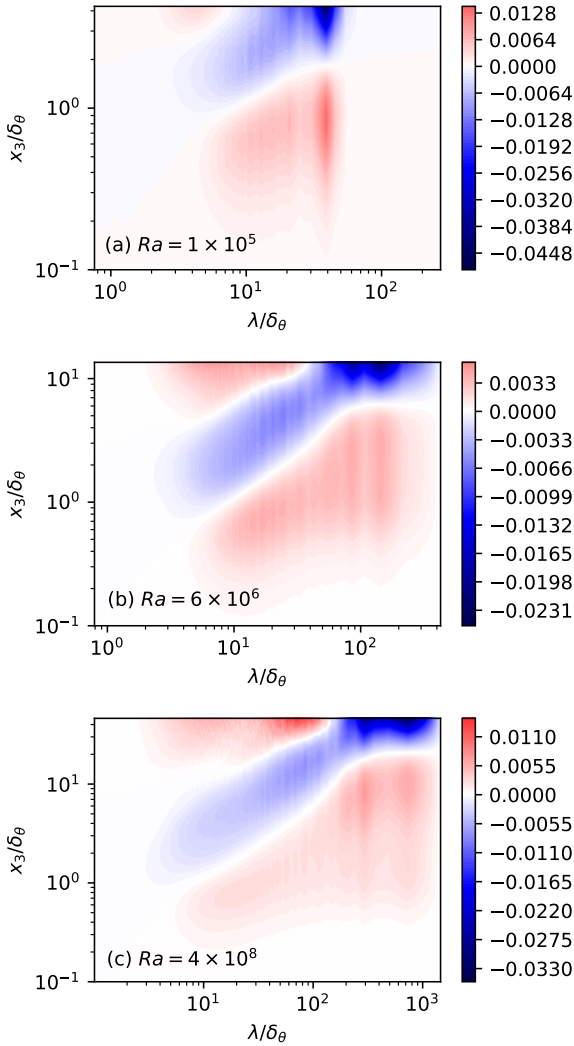


Figure 7. k - and x_3 -Premultiplied spectral density of \mathcal{N}_K

CONCLUSION

In this work, we apply spectral analysis to the terms in the TKE transport equation. The production and dissipation are mostly concentrated at the middle point between walls. However, their dominant length scales are different. The inter-scale transfer mechanism is mostly responsible for such scale separation between production and dissipation. In the cascade pro-

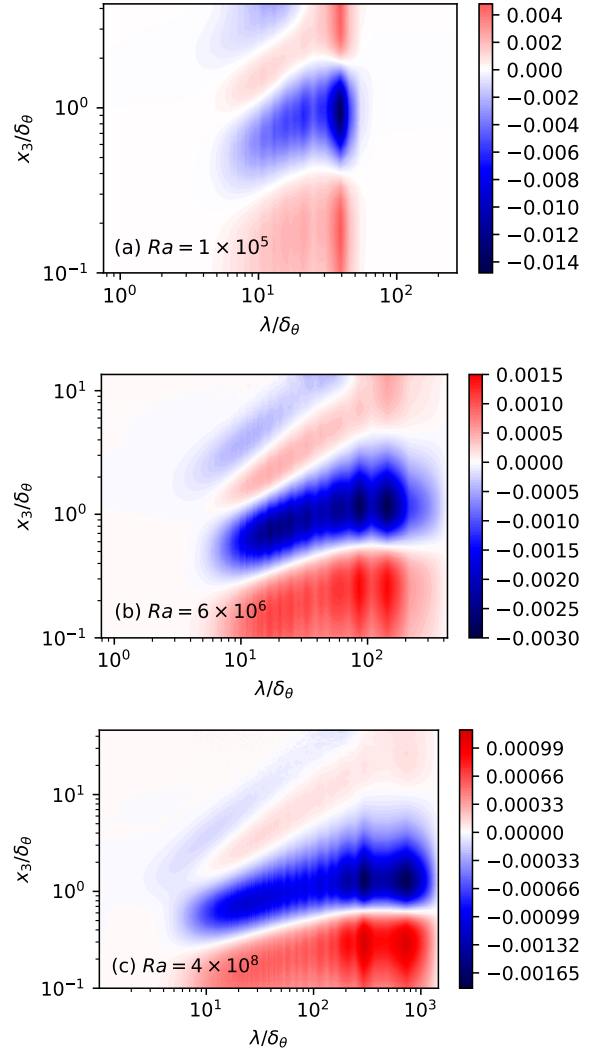


Figure 8. k - and x_3 -Premultiplied spectral density of D_K

cess of TKE from the large-scale to the small-scale, some TKE gets transported toward walls and then transported away from the wall.

In the early part of this work, we speculate the existence of bi-modal spectral peaks of TKE at high Ra flows, but it is unable to verify it because it could be an artifact of a small simulation domain. Even though it is at the different wall-normal locations, the inter-scale transfer also shows the bimodal peaks in the donor region at high Ra flows. We speculate that these two bimodal behavior at high Ra flows is connected, but, again, we may need to have simulation results with a larger simulation domain and perhaps higher Ra flows.

There are several future works. First, we need a better scaling parameter than δ_θ and h . δ_θ successfully describes the scaling of dissipation at the middle point between walls. Other than that, we are unable to find any invariant scaling with δ_θ in flows at different Ras even in the near-wall region. Second, this work is limited to the TKE, but each component of TKE should be studied. Especially, the wall-normal velocity component is the only one with a non-zero production mechanism. Therefore, inter-component energy transfer should have an important role in the life-cycle of TKE. Third, we can apply the same analysis techniques to the temperature fluctuations and velocity-temperature correlations. The velocity-temperature correlation is particularly important because it is a production

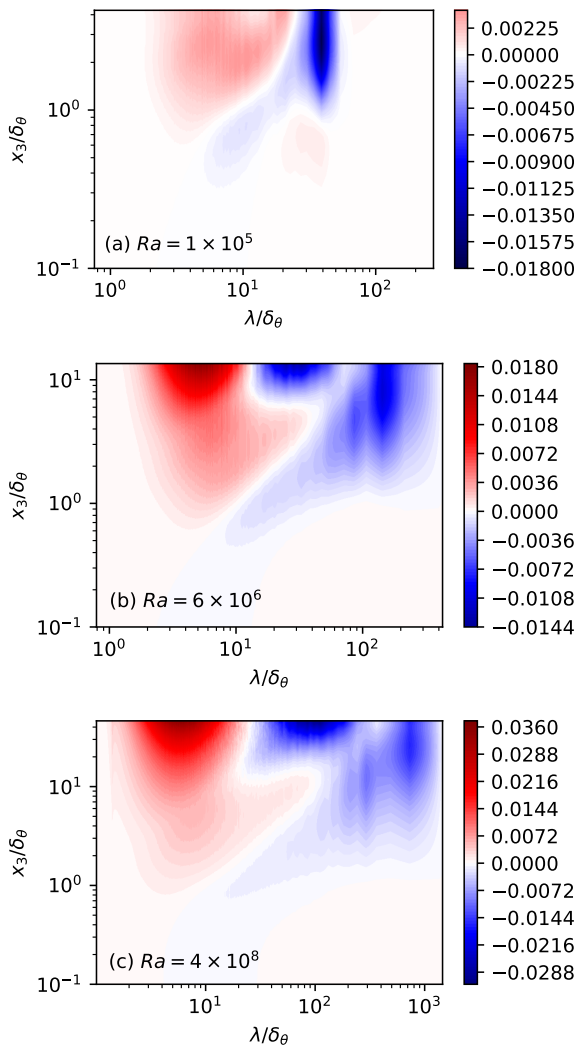


Figure 9. k - and x_3 -Premultiplied spectral density of T_k^{\parallel}

mechanism of TKE. Yet, the analysis of velocity-temperature correlation is challenging because it requires studies not only on the magnitude but also on the phase in the spectral densities of budget terms. Finally, we limited our simulation cases with unity Pr in this work. The effect of Pr must be investigated.

ACKNOWLEDGEMENT

This research used resources of the Argonne Leadership Computing Facility, which is a DOE Office of Science User Facility supported under Contract DE-AC02-06CH11357.

REFERENCES

Ahlers, Guenter, Grossmann, Siegfried & Lohse, Detlef 2009 Heat transfer and large scale dynamics in turbulent

Rayleigh-Bénard convection. *Reviews of Modern Physics* **81** (2), 503–537.

Blass, Alexander, Verzicco, Roberto, Lohse, Detlef, Stevens, Richard J.A.M. & Krug, Dominik 2021 Flow organization in laterally unconfined Rayleigh-Bénard turbulence. *Journal of Fluid Mechanics* **906**, A26.

Deardorff, J. W. & Willis, G. E. 1967 Investigation of turbulent thermal convection between horizontal plates. *Journal of Fluid Mechanics* **28** (4), 675–704.

Green, Gerrit, Vlaykov, Dimitar G, Mellado, Juan Pedro & Wilczek, Michael 2020 Resolved energy budget of superstructures in Rayleigh-Bénard convection. *Journal of Fluid Mechanics* **887**, A21.

Kerr, R. M. 2001 Energy Budget in Rayleigh-Bénard Convection. *Physical Review Letters* **87** (24), 244502.

Kim, John, Moin, Parviz & Moser, Robert 1987 Turbulence statistics in fully developed channel flow at low reynolds number. *Journal of Fluid Mechanics* **177**, 133–166.

Krug, Dominik, Lohse, Detlef & Stevens, Richard J. A. M. 2020 Coherence of temperature and velocity superstructures in turbulent rayleigh-bénard flow. *Journal of Fluid Mechanics* **887**, A2.

Lee, Myoungkyu, Malaya, Nicholas & Moser, Robert D. 2013 Petascale direct numerical simulation of turbulent channel flow on up to 786k cores. In *SC13, the International Conference for High Performance Computing, Networking, Storage and Analysis*, pp. 1–11.

Lee, Myoungkyu & Moser, Robert D. 2015 Direct numerical simulation of turbulent channel flow up to $Re_\tau \approx 5200$. *Journal of Fluid Mechanics* **774**, 395–415.

Lee, Myoungkyu & Moser, Robert D. 2018 Extreme-scale motions in turbulent plane couette flows. *Journal of Fluid Mechanics* **842**, 128–145.

Lee, Myoungkyu & Moser, Robert D. 2019 Spectral analysis of the budget equation in turbulent channel flows at high reynolds number. *Journal of Fluid Mechanics* **860**, 886–938.

Lee, Myoungkyu, Ulerich, Rhys, Malaya, Nicholas & Moser, Robert D. 2014 Experiences from leadership computing in simulations of turbulent fluid flows. *Computing in Science Engineering* **16** (5), 24–31.

Orszag, Steven A. 1971 On the elimination of aliasing in finite-difference schemes by filtering high-wavenumber components. *Journal of the Atmospheric Sciences* **28**, 1074.

Pandey, Ambrish, Scheel, Janet D. & Schumacher, Jörg 2018 Turbulent superstructures in rayleigh-bénard convection. *Nature Communications* **9** (1), 1–11.

Stevens, Richard J A M, Blass, Alexander, Zhu, Xiaojue, Verzicco, Roberto & Lohse, Detlef 2018 Turbulent thermal superstructures in Rayleigh-Bénard convection. *Physical Review Fluids* **3** (4), 041501(R).